

The Effect of Dust Extinction on the Observed Properties of Galaxies in the Near-Infrared.

Ihab F. Riad,¹ Renée C. Kraan-Korteweg¹ and Patrick A. Woudt¹

¹*Department of Astronomy, University of Cape Town, Private Bag, X3 Rondebosch 7701, South Africa*

ABSTRACT

Galaxies behind the Milky Way suffer size reduction and dimming due to their obscuration by dust in the disk of our Galaxy. The degree of obscuration is wavelength dependent. It decreases towards longer wavelengths. Compared to the optical, the Near InfraRed (NIR) K_s band extinction is only $\approx 10\%$ that of the B band. This makes NIR surveys well suited for galaxy surveys close to the Galactic Plane where extinction is severe.

While Galactic obscuration is less prominent in the NIR it is not negligible. In this paper we derive empirical relations to correct isophotal radii and magnitudes of galaxies observed in the NIR for foreground absorption. We simulate extinction in the J , H and K_s bands on 64 (unobscured) galaxies from the 2MASS Large Galaxy Atlas (Jarrett et al. 2003). We propose two methods for the extinction correction, the first is optimized to provide the most accurate correction and the second provides a convenient statistical correction that works adequately in lower extinction regions. The optimized correction utilizes the galaxy surface brightness, either the disk central surface brightness, μ_0 , or the combined disk plus bulge central surface brightness, elliptical and disk/spiral Hubble types. A detailed comparison between the different methods and their accuracy is provided.

Key words: galaxies: photometry - infrared:galaxies - dust, extinction.

1 INTRODUCTION

The effect of dust extinction on point-like objects, stars, is linearly related to extinction. If, for example, the observed magnitude of a star is $K_s = 6^m0$ and it suffers an extinction of $A_{K_s} = 1^m5$, its intrinsic magnitude will be $K_s^\circ = 4^m5$. Extended objects, like galaxies, suffer a further dimming due to the loss of their fainter outer regions in the sky background. An obscured galaxy appears smaller and fainter in the sky than it really is. Corrections for this extra dimming are non-linear as was shown by Fisher & Tully (1981); Hauschildt (1987) and Cameron (1990) in the optical. Nagayama et al. (2004) derived corrections to the K_s band isophotal magnitudes. Their extinction correction study was initiated to correct the isophotal magnitudes for galaxies observed in the vicinity of the giant radio galaxy PKS 1343-601 centred at $(\ell, b) = (309^\circ7, 1^\circ7)$. The average extinction in their region was $A_{K_s} \lesssim 1^m1$. From their study they showed that the isophotal magnitude correction can be approximated by a linear relation for extinction levels $A_{K_s} \lesssim 1^m0$. Their work also showed that the different morphological types of galaxies are affected differently by extinction. Galaxies that have an exponential light profile bulge (late type) need larger corrections than those with a de Vaucouleurs profile (early type), or those with a bulge+disk light profile.

Statistical results and conclusions derived from magnitude-limited and radius-limited galaxy catalogues are unreliable if they are not corrected for these extinction effects. Applying extinction corrections to galaxy catalogues like the 2MASS Extended Source

Catalog (2MASX) (Jarrett et al. 2000) will imply fainter completeness magnitudes than the currently quoted values. Applying extinction corrections to optical catalogues for galaxies observed in the Zone of Avoidance (ZOA) helped reduce the optical ZOA from the region with extinction $A_B \lesssim 1^m0$, to the region with $A_B \lesssim 3^m0$ (Kraan-Korteweg & Lahav 2000). This reduction was a result of including those galaxies that did not make it into the diameter limited catalogues if they were not corrected for extinction.

Extinction magnitude corrections are crucial when relating spiral galaxy magnitudes to their velocity width for the Tully-Fisher (TF) relation. The here derived NIR extinction corrections will prove invaluable for e.g. the ongoing whole-sky 2MASS Tully Fisher Survey (Masters et al. 2008), especially for galaxies found in the ZOA. Application of NIR magnitude extinction corrections will also improve photometric redshift estimations (Jarrett 2004) for galaxies that are observed in the ZOA.

Motivated by an ongoing NIR imaging survey to map the crossing of the Great Attractor wall across the ZOA where extinction levels are severe, we initiated a study of the effect of Galactic extinction on galaxies imaged in the $J(1.2\mu m)$, $H(1.6\mu m)$ and $K_s(2.2\mu m)$ bands. This will allow us to correct their observed isophotal-radii and magnitudes for extinction. In our current ZOA survey along the Norma wall (Riad et al., in preparation) we noticed, that $\approx 85\%$ of the galaxies in our sample were found in regions with an extinction $A_J \lesssim 1^m0$, while $\approx 14\%$ were found in regions with an extinction $1^m0 \lesssim A_J \lesssim 3^m0$. Only 1% of the galaxies were found in regions with an extinction $A_J > 3^m0$. For

the H and K_s band $\approx 94\%$ and 98% respectively of the galaxies were found in regions with $A_{H,K_s} \lesssim 1^m0$, while $\approx 5\%$ and 1% of the galaxies were obscured by $1^m0 \lesssim A_{H,K_s} \lesssim 3^m0$. Only a handful of the galaxies were found in regions with $A_{H,K_s} > 3^m0$. We therefore limited the simulation to the extinction range $A_{J,H,K_s} = 0^m0 - 3^m0$. In this work and for the purpose of estimating the extinction suffered by galaxies in our ZOA survey we used the general extinction law,

$$\frac{A_V}{E(B-V)} = R_V.$$

Where $E(B-V)$ is the colour reddening derived from the Schlegel et al. (1998) reddening maps and A_V is the extinction in the optical V band. A typical value for R_V is 3.1 (Cardelli et al. 1989). Extinction in the NIR J , H and K_s passbands was derived using the parametrization given by Cardelli et al. (1989), see Eqs. 1 - 3.

$$A_J = 0.874 E(B-V), \quad (1)$$

$$A_H = 0.549 E(B-V), \quad (2)$$

$$A_{K_s} = 0.365 E(B-V). \quad (3)$$

In this paper, we derive NIR corrections to isophotal magnitudes and radii for galaxies obscured by the Milky Way. Section 2 describes the data set and method. We describe two methods to apply the corrections (Sects. 2.2 and 2.3). In Sect. 3 we provide a brief comparison between the different methods, and discuss their respective reliability.

2 DATA AND METHOD

We selected 64 galaxies from the 2MASS Large Galaxy Atlas (LGA) (Jarrett et al. 2003) to simulate the effect of extinction on isophotal-radii and magnitude for galaxies observed in the NIR. 2MASS is an All-Sky NIR survey in the bands $J(1.2 \mu m)$, $H(1.6 \mu m)$ and $K_s(2.2 \mu m)$. Galaxies were selected in such a way that they are minimally affected by contamination from neighbouring sources, and give a fair representation of all morphological types. The sample includes 25 elliptical and lenticular (**E/S0**), and 39 spiral (**S**) galaxies. Half of the galaxies in the spiral galaxy sample are barred with some of them having ring features. The selected galaxies cover a wide range in galaxy size and brightness. The apparent radii range between $r_{20} = 34'' - 1614''$ where r_{20} is the isophotal radius at the surface brightness level $\mu_K = 20 \text{ mag/arcsec}^2$. The apparent isophotal magnitude range covered by our sample is $K_{20} = 1^m04 - 10^m77$, where K_{20} is the integrated magnitude within r_{20} . The galaxies in our sample suffered minimal obscuration ranging between $A_{K_s} = 0^m01 - 0^m07$, see last column in Table 1. The list of selected galaxies is given in Table 1. This table lists the most common name of the galaxy, followed by the morphological type, r_{20} , K_{20} , inclination (b/a) and position angle (PA) in the K_s band. All the data are taken from Jarrett et al. (2003). In the table we also give the disk central surface brightness μ_0 (Freeman 1970) and the central surface brightness μ_c in the K_s band. The last column lists the mean extinction A_{K_s} . Extinction in the K_s band was derived from the Schlegel et al. (1998) reddening maps and Eqn. 3. The surface brightness profiles for the galaxies are taken from the LGA¹ (given in tabular format).

¹ The surface brightness profile for galaxies in the LGA are found in <http://irsa.ipac.caltech.edu/applications/2MASS/LGA/>

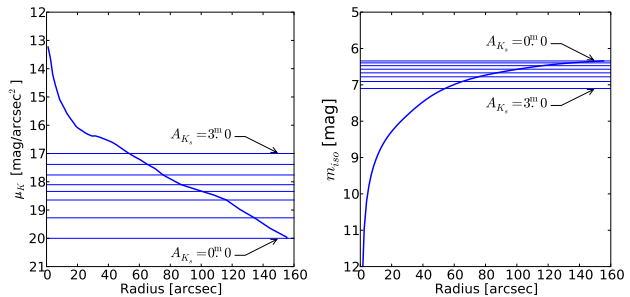


Figure 1. The effect of extinction on the spiral galaxy M88. Left panel: surface brightness profile for M88 in the K_s band, with various levels of the simulated extinction in the range $A_{K_s} = 0^m0$ to 3^m0 . Right panel: integrated isophotal magnitude m_{iso} with extinction with the same levels of the simulated extinction.

The method we implement here for simulating the effect of extinction on galaxies closely follows the precepts of earlier work done by Cameron (1990) in the B -band.

It is difficult to define a reliable total radius and magnitude for a galaxy (Jarrett et al. 2003), but more straightforward to work with isophotal radii and magnitudes out to a given radius. For this reason we only consider here corrections to isophotal radii and the flux within that respective radius. In this paper, we define the limiting isophotal radius R as the radii to an isophote of $21.4 \text{ mag/arcsec}^2$ in the J , $20.6 \text{ mag/arcsec}^2$ in the H , and 20 mag/arcsec^2 in the K_s band. Those values are approximately the 1σ NIR sky background (Jarrett et al. 2003). We also define the integrated isophotal magnitude m_{iso} as the integrated magnitude out to this radius R .

2.1 Simulating extinction

The simulation of the effect of Galactic extinction on the apparent properties of a galaxy was achieved by the inward displacement of the limiting isophote along the surface brightness profile. The limiting isophote was shifted in non-uniform steps along the galaxy light profile with each step being equivalent to a certain extinction level in the investigated band. As an example, the left panel of Fig. 1 shows the effect of extinction on the surface brightness profile of the spiral galaxy M88 in the K_s band. The panel indicates increasing levels of extinction at $A_{K_s} = 0^m0, 0^m7, 1^m4, 1^m7, 1^m9, 2^m2, 2^m6$ and $A_{K_s} = 3^m0$ applied to the galaxy. The extinction levels are represented as horizontal lines on the plots. For each of the horizontal lines, the part of the profile lying below the line represents the obscured part of the galaxy while the part above is what remains visible at a given extinction. The intercept of the line with the ordinate gives the apparent limiting isophote, while the intercept of the light profile on the abscissa shows the size of the obscured galaxy that remains visible. The projection of the point of intercept of the line representing $A_{K_s} = 0^m0$ with the light profile on the abscissa gives the intrinsic radius R° . The additional dimming caused by the loss of the faint outer region is demonstrated by the integrated isophotal magnitude profile m_{iso} shown in Fig. 1 (right panel).

The reduced radii and magnitudes were calculated for each step and compared to the original values. The quantities calculated

Table 1. The sample of galaxies used for the study of extinction effects on the NIR.

No.	Galaxy	Morphology	r_{20} [$''$]	K_{20} [mag]	b/a	PA [$^{\circ}$]	μ_0 [mag/arcsec 2]	μ_c [mag/arcsec 2]	A_{K_s} [mag]
1	NGC4697	E6	123.8	6.502	0.63	+67.5	16.10	12.88	0.011
2	M86	S03/E3	151.4	6.283	0.67	-55.0	16.37	13.21	0.011
3	M60	E2	146.6	5.825	0.81	-72.5	15.83	13.06	0.010
4	M59	E5	109.0	6.866	0.65	-15.0	16.11	12.67	0.012
5	M84	E1	115.0	6.347	0.92	-57.5	16.12	12.93	0.015
6	M105	E1	108.0	6.362	0.85	+67.5	15.92	12.65	0.009
7	NGC584	E4	88.8	7.445	0.62	+62.5	16.18	13.05	0.015
8	NGC720	E5	90.5	7.396	0.55	-40.0	16.14	13.63	0.006
9	NGC1395	E2	93.7	7.024	0.82	-87.5	16.10	13.29	0.008
10	NGC1407	E0	100.2	6.855	0.95	+60.0	16.25	13.62	0.025
11	NGC4365	E3	113.0	6.800	0.74	+45.0	16.32	13.36	0.008
12	NGC4473	E5	93.7	7.269	0.54	-85.0	15.96	12.89	0.010
13	NGC4494	E1-2	91.1	7.145	0.87	-07.5	16.15	13.04	0.009
14	NGC4589	E2	69.5	7.915	0.75	+92.5	16.27	13.67	0.010
15	NGC1377	S0	35.0	9.892	0.56	-86.5	16.15	15.43	0.010
16	NGC2310	S0	91.5	8.565	0.24	+47.0	15.97	14.99	0.039
17	NGC3630	S0	42.2	8.911	0.45	+37.0	15.70	13.46	0.016
18	NGC3966	S0	61.5	9.077	0.24	-72.5	15.75	14.63	0.011
19	NGC3115	S0	164.6	5.937	0.39	+45.0	15.74	12.27	0.017
20	NGC4636	E/S0;1	134.8	6.628	0.84	-37.5	16.36	13.82	0.010
21	NGC1340	E5	86.0	7.546	0.62	-17.5	16.01	13.58	0.007
22	M49	E2/S0(2)	179.2	5.506	0.81	-17.5	16.11	12.98	0.008
23	M32	cE2	147.4	5.139	0.87	+15.0	14.96	11.11	0.023
24	M87	E+0-1;pec;Sy	136.0	5.904	0.86	+27.5	16.05	13.64	0.008
25	NGC855	E	41.6	10.161	0.50	+67.0	16.71	15.97	0.026
26	NGC4244*	SA(s)cd	157.0	8.110	0.30	+45.5	17.49	16.82	0.008
27	NGC55*	SB(s)m	273.5	6.562	0.30	-67.0	17.12	17.03	0.005
28	NGC1073*	SB(rs)c	57.7	9.690	0.72	+42.5	18.70	16.99	0.014
29	NGC247*	SAB(s)d	141.7	8.180	0.55	+01.5	18.21	17.01	0.007
30	NGC24*	SA(s)c	83.0	9.215	0.28	+43.5	16.97	17.03	0.007
31	M33*	SA(s)cd	499.9	5.38	0.80	+50.5	17.71	14.10	0.015
32	NGC4569	SAB(rs)ab;Sy	165.1	7.686	0.40	-15.0	16.35	12.83	0.017
33	NGC4216	SAB(s)b	217.6	6.587	0.80	+109.5	15.76	12.97	0.012
34	M100	SAB(s)bc;LINER	150.8	6.810	0.73	-72.5	17.28	13.97	0.010
35	M106	SAB(s)b;LINER	263.9	5.598	0.49	-20.0	15.98	13.39	0.006
36	M51a	SA(s)bc	197.5	5.601	0.68	+57.5	16.38	13.57	0.013
37	M109	SAB(rs)bc;LINER	142.6	7.139	0.56	+38.0	17.17	14.02	0.010
38	NGC908	SA(s)c	128.9	7.365	0.55	+87.5	16.41	14.54	0.009
39	NGC488	SA(r)b	107.8	7.133	0.81	+05.0	16.45	13.81	0.011
40	NGC4826	SA(rs)ab;Sy2	214.8	5.396	0.57	-70.0	15.24	12.38	0.015
41	NGC4594	SA(s)a;Sy1.9	201.7	5.009	0.54	+87.5	16.35	11.87	0.019
42	NGC474	SA(s)0	46.1	8.815	0.99	+45.0	16.42	14.05	0.013
43	NGC1532	SB(s)b;pec;sp	143.6	6.861	0.30	+35.0	15.92	13.84	0.006
44	NGC7090	SBc?;sp	136.4	8.404	0.26	-48.0	17.13	13.65	0.008
45	NGC2442	SAB(s)bc;pec	126.4	7.071	0.87	+27.5	17.04	13.61	0.074
46	M51b	SB0;pec	124.2	6.402	0.99	+27.5	15.77	12.33	0.013
47	NGC1808	SAB(s)bc;Sy2	131.1	6.732	0.42	-37.0	15.78	12.77	0.011
48	NGC5005	SAB(rs)bc;Sy2	130.8	6.501	0.42	+67.5	15.25	12.84	0.005
49	M88	SA(rs)b	155.4	6.334	0.44	-40.0	15.56	13.24	0.014
50	NGC4527	SAB(s)bc	141.0	7.021	0.34	+69.5	15.60	12.89	0.008
51	M63	SA(rs)bc	204.2	5.728	0.58	-82.5	15.76	12.71	0.006
52	M98	SA(s)ab,III	172.8	7.012	0.34	+69.5	16.54	13.38	0.013
53	NGC47	SB(rs)bc	33.8	9.988	0.55	+85.5	17.12	15.49	0.004
54	NGC210	SA(s)b	54.1	8.515	0.52	-07.5	15.85	14.21	0.008
55	NGC628	SA(s)c	125.3	7.187	0.86	+87.5	17.53	15.47	0.026
56	NGC772	SA(s)b	105.2	7.440	0.80	-45.0	16.64	14.08	0.027
57	NGC1187	SB(r)c	86.1	8.315	0.55	+52.5	17.18	14.28	0.008
58	NGC522	Sc	68.9	9.389	0.14	+33.0	15.45	15.67	0.032
59	NGC891	SA(s)b	225.4	5.994	0.24	+25.0	15.11	14.55	0.024
60	M31	SA(s)b	1614.0	1.038	0.56	+45.0	14.81	11.50	0.023
61	NGC5746	SAB(rs)b?;sp	162.2	6.927	0.26	-10.0	15.10	14.08	0.015
62	M94	SA(r)ab	172.3	5.169	0.79	+85.0	15.50	11.70	0.007
63	NGC1300	SB(s)bc	131.8	7.896	0.48	-79.0	17.63	14.26	0.011
64	M65	SAB(rs)a	211.6	6.113	0.32	-08.5	14.95	13.312	0.009

The table lists the morphological type, r_{20} , K_{20} , (b/a) and PA, values are taken from the LGA (Jarrett et al. 2003). The table also lists the K_s band μ_0 and μ_c . Extinction in the K_s band is also listed. Galaxies marked with * are those showing the deviated correction trend explained in the next section.

as a function of extinction were $f(R)$ and Δm_{iso} , defined as,

$$f(R) = \frac{R^{\circ}}{R},$$

$$\Delta m_{iso} = m_{iso} - m_{iso}^{\circ},$$

where m_{iso}° , m_{iso} , R° and R are the intrinsic and absorbed mag-

nitudes and radii respectively. The different values of $f(R)$ and Δm_{iso} corresponding to the simulated extinction values were then calculated, and fitted to the empirical relations following the for-

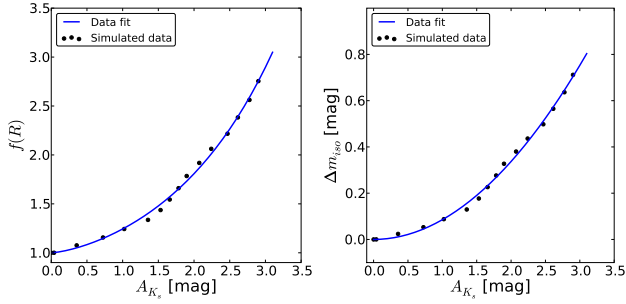


Figure 2. The calculated $f(R)$ (left), and Δm_{iso} (right), with their fitted corrections for the spiral galaxy M88 in the K_s band.

malism given by Cameron (1990):

$$f(R) = 10^{a \cdot (A_\lambda)^b}, \quad (4)$$

$$\Delta m_{iso} = F \cdot (A_\lambda)^v, \quad (5)$$

where F , v , a , b are the fitting parameters, and A_λ the extinction. This parameter fitting was done for all galaxies in our sample. It was performed separately for all three J , H , K_s bands.

The resulting corrections show very comparable trends in the three bands, due to the similarity of the light profiles of the galaxy in the three bands. To demonstrate the effectiveness of our procedure we therefore reduce the discussion to the results of the K_s band only. Figure 2 displays the calculated values of $f(R)$, and Δm_{iso} as a function of A_{K_s} , with their fitted relations for the galaxy M88 in the K_s band. The ability of Eqns. 4, 5 to fit the simulated data varies among the galaxies. Some galaxies show tighter fits compared to M88, while others show more dispersion. The variation in the quality of the fitting is expected due to the different structures imprinted on the surface brightness profile of the galaxies.

2.2 Variation among galaxies (optimized corrections)

In Fig. 3 we show the magnitudes and radii corrections for all the **E/S0** (top), and **S** galaxies (bottom). The curves in the plots clearly show that the Cameron (1990) relations in their present form can not fully account for the variation among the galaxies in the two respective groups.

We investigated the origin of these discrepancies by looking at trends with e.g. inclination, central surface brightness μ_c , and the disk central surface brightness μ_0 extrapolated from the fainter outer disk. No significant trend was found between the corrections and the variation among galaxies inclinations. Most probably a much larger sample than the current one is needed to investigate the correlation. A clear correlation between μ_0 and μ_c with the corrections was noticed, however.

It was noted that galaxies with a low central surface brightness $\mu_c \geq 17.0$ mag/arcsec² in the K_s band, and low surface brightness galaxies in general require larger corrections. This is expected as those galaxies become obscured much more quickly. Galaxies that required larger corrections in our sample are M33, NGC24, NGC247, NGC1073, NGC55, NGC4244; they are labeled in Fig. 3. Even though the corrections were found to depend on μ_c , it was in fact found that μ_0 shows the better correlation with the corrections.

In this section we describe the method to optimize the corrections using either μ_0 or μ_c . Optimizing the corrections using μ_0

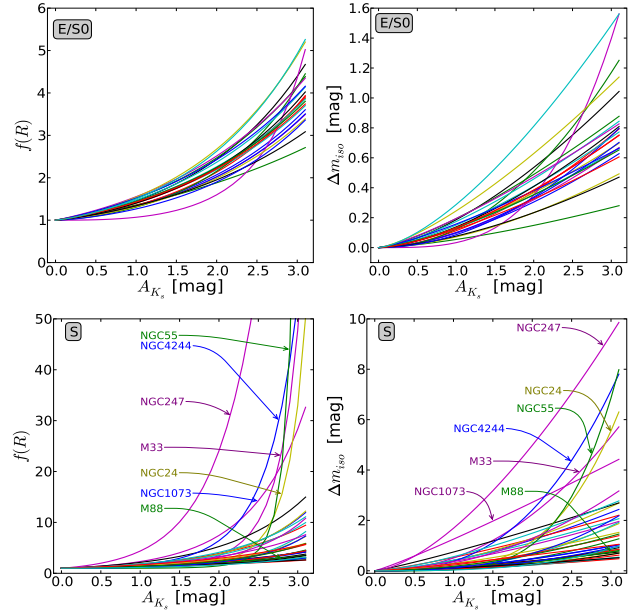


Figure 3. Simulated corrections $f(R)$ and Δm_{iso} . **E/S0** top panel, **S** bottom panel.

gives tighter estimates to the corrections than using μ_c . On the other hand, optimizing the corrections using μ_c is convenient since it is easily measured and is typically found in large catalogues including 2MASX. A further point to note is that the NIR μ_c can be used to roughly classify the galaxies as early or late-type galaxies (Jarrett 2000). In Sect. 2.3 we derive a more general correction which can be applied when only the galaxies are classified as early or late type but neither μ_0 nor μ_c is available.

2.2.1 Optimized correction based on μ_0

It was realized that the derived quantity, μ_0 , defined as the disk central surface brightness extrapolated from the fainter outer regions of the galaxy correlates well with the deviation among the galaxies. The definition of μ_0 corresponds to the disk central surface brightness for spirals as defined by Freeman (1970). The better correlation of the corrections with μ_0 rather than μ_c is expected since it is always the fainter outer regions of the galaxy that suffer most from extinction. To accommodate μ_0 into the corrections, Eqns. 4, 5 were re-written as,

$$f(R, \mu_0) = 10^{a(\mu_0) \cdot (A_\lambda)^{b(\mu_0)}}, \quad (6)$$

$$\Delta m_{iso}(\mu_0) = F(\mu_0) \cdot (A_\lambda)^{v(\mu_0)}, \quad (7)$$

with

$$\begin{aligned} a(\mu_0) &= a_\circ \exp(\mu_0 \cdot a_1), \\ b(\mu_0) &= b_\circ \exp(\mu_0 \cdot b_1), \\ F(\mu_0) &= F_\circ \exp(\mu_0 \cdot F_1), \\ v(\mu_0) &= v_\circ \exp(\mu_0 \cdot v_1). \end{aligned} \quad (8)$$

Using the parameter products $(a \times b)$, $(F \times v)$ for each galaxy, and analyzing how they vary with μ_0 , we derived these parameters $(a_\circ, b_\circ, F_\circ, v_\circ, a_1, b_1, F_1, \text{ and } v_1)$. The values are listed in Table 2. For each galaxy, the value of μ_0 was found from a linear fitting to the disk part of the light profile of the galaxy with $\mu_\lambda \gtrsim 17.0$

Table 2. Parameters a_o , b_o , F_o , v_o , a_1 , b_1 , F_1 , and v_1 for the μ_0 optimization Eqn. 8

Galaxy	Param.	J	H	K_s
E/S0	a_o	0.0005	$5.2(e^{-06})$	0.0002
	a_1	0.3301	0.6248	0.3993
	b_o	0.3659	15.9697	1.9398
	b_1	0.0704	-0.1589	-0.0289
	F_o	$2.8(e^{-11})$	$1.5(e^{-11})$	$6.7(e^{-11})$
	F_1	1.3090	1.3912	1.3309
	v_o	8.1329	236.9696	18.9573
	v_1	-0.0979	-0.3075	-0.1561
S	a_o	$3.3(e^{-06})$	$3.9(e^{-06})$	0.0001
	a_1	0.6093	0.6203	0.4406
	b_o	9.7884	7.0789	2.6909
	b_1	-0.1116	-0.095	-0.0395
	F_o	$8.1(e^{-11})$	$1.4(e^{-10})$	$2.4(e^{-7})$
	F_1	1.2277	1.2443	0.8365
	v_o	201.5666	56.9891	17.5403
	v_1	-0.2693	-0.2055	-0.1415

Table 3. Parameters a_o , b_o , F_o , v_o , a_1 , b_1 , F_1 , and v_1 for the μ_c optimization Eqn. 11

Galaxy	Param.	J	H	K_s
E/S0	a_o	0.1279	0.0547	0.1598
	a_1	0.0063	0.0707	-0.0061
	b_o	0.8397	1.3805	0.7292
	b_1	0.0248	-0.0115	0.0381
	F_o	0.0073	0.0034	0.0151
	F_1	0.1889	0.2574	0.1632
	v_o	1.4504	2.1299	0.8602
	v_1	0.0046	-0.0253	0.0420
S	a_o	0.0068	0.0095	0.0157
	a_1	0.1953	0.1824	0.1641
	b_o	2.7721	2.5213	1.3653
	b_1	-0.0455	-0.0397	0.0009
	F_o	0.0003	0.0007	0.0012
	F_1	0.4136	0.3833	0.3751
	v_o	6.4910	4.6215	2.3296
	v_1	-0.0866	-0.0674	-0.0267

mag/arcsec². The intercept of the straight line fitted to the disk part of the light profile with the surface brightness axis was then μ_0 . The disk part of the light profile was identified by visual inspection.

The goodness of $f(R, \mu_0)$ and Δm_{iso} in describing the correction curves for the different galaxies accurately was found to be very sensitive to the value of μ_0 . This shows the importance of having an accurate light profile of the galaxies, and hence μ_0 , to be able to use the μ_0 optimized correction.

2.2.2 Optimized correction based on μ_c

For optimizing the extinction corrections using the central surface brightness μ_c we used the same methodology as for the μ_0 optimization. To incorporate μ_c in the corrections we re-wrote Eqns. 4 and 5 as,

$$f(R, \mu_c) = 10^{a(\mu_c) \cdot (A_\lambda)^{b(\mu_c)}}, \quad (9)$$

$$\Delta m_{iso}(\mu_c) = F(\mu_c) \cdot (A_\lambda)^{v(\mu_c)}, \quad (10)$$

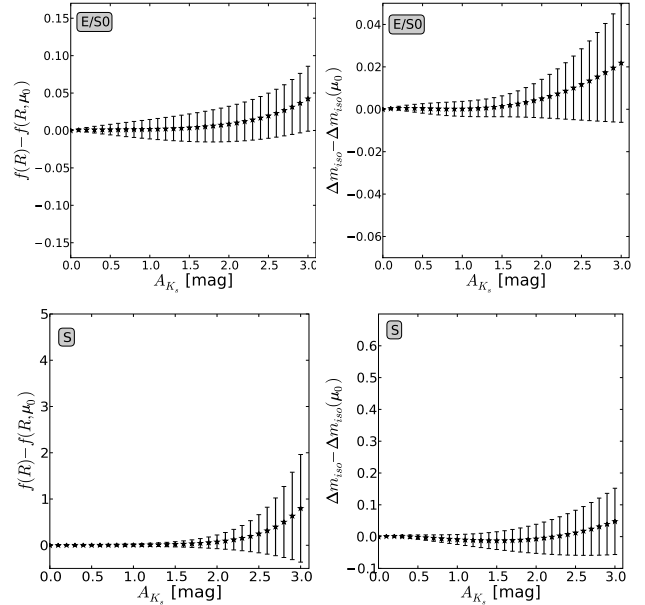
with

$$\begin{aligned} a(\mu_c) &= a_o \exp(\mu_c \cdot a_1), \\ b(\mu_c) &= b_o \exp(\mu_c \cdot b_1), \\ F(\mu_c) &= F_o \exp(\mu_c \cdot F_1), \\ v(\mu_c) &= v_o \exp(\mu_c \cdot v_1). \end{aligned} \quad (11)$$

Again we determine the products ($a \times b$) and ($F \times v$) and how they vary with μ_c and hence derived the parameters ($a_o, b_o, F_o, v_o, a_1, b_1, F_1$, and v_1). The values of these parameters are given in Table 3.

To quantify the performance of the two optimization corrections, we computed the difference between the corrections as given by the simulated data and as given by the optimized corrections using both the parametrization $f(R, \mu_0)$, $\Delta m_{iso}(\mu_0)$ and using $f(R, \mu_c)$, $\Delta m_{iso}(\mu_c)$. The comparison was made for all galaxies in the K_s band in the extinction range $A_{K_s} = 0^m0 - 3^m0$. A summary of the comparisons is listed in Table 4, and displayed in Fig. 4 for the μ_0 optimization, and Table 5, Fig. 5 for the μ_c optimization.

The error bars in Figs. 4, 5 and the plots that follow are the


Figure 4. Comparison between simulated corrections and μ_0 optimised corrections derived using $f(R, \mu_0)$ and $\Delta m_{iso}(R, \mu_0)$, top: E/S0, bottom: S galaxies.

standard deviation error defined as $SDE = \sigma/\sqrt{N}$, with σ , the standard deviation of the binned values and N the number of data points in the bin, which are 25 for E/S0, and 39 for S.

The plots and tables show that the accuracy of the corrections are extinction dependent, showing smaller deviations and less dispersion at low levels of extinction. It is also evident that spiral galaxies show larger deviations and more dispersion than elliptical and lenticular galaxies. The relatively larger errors for the spiral galaxies can be attributed to the more structural features like spiral arms, bars traced by their light profiles. The comparison also shows that the corrections parametrized using the disk central surface brightness show less systematic shifts and tighter dispersion

Table 4. Comparison between simulated corrections and μ_0 optimized corrections at the extinction levels $A_{K_s} = 0^m5, 1^m0, 2^m0$ and 3^m0 .

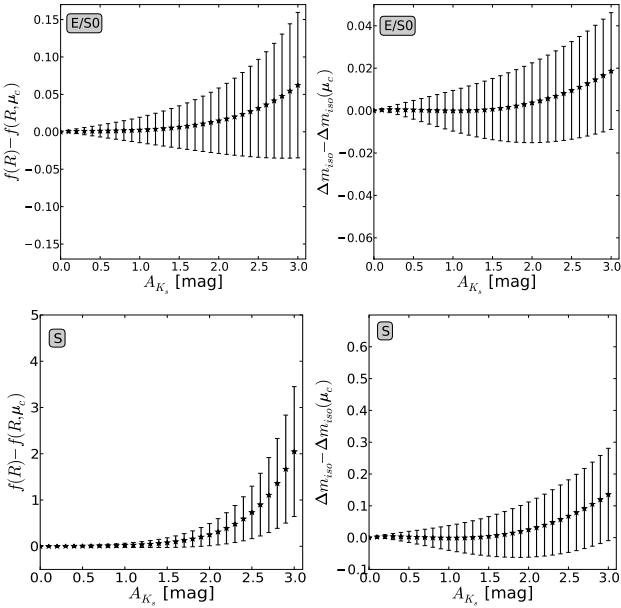
Galaxy	Param.	0^m5	<i>SDE</i>	1^m0	<i>SDE</i>	2^m0	<i>SDE</i>	3^m0	<i>SDE</i>
E/S0	$f(R)$	0.0012	0.0071	0.0017	0.0130	0.0087	0.0236	0.0424	0.0433
E/S0	Δm_{iso}	0.0004	0.0022	0.0002	0.0035	0.0050	0.0091	0.0218	0.0280
S	$f(R)$	0.0042	0.0104	0.0071	0.0248	0.0748	0.1476	0.7993	1.1632
S	Δm_{iso}	-0.0016	0.0069	-0.0090	0.0156	-0.0070	0.0457	0.0479	0.1042

The μ_0 optimized corrections were calculated using Eqns. 6, 7. The value of μ_0 for each galaxy was found by performing a linear regression to fainter outer region of the galaxy light profile with $\mu_\lambda \gtrsim 17.0$ mag/arcsec² and measuring its intercept with the ordinate.

Table 5. Comparison between simulated corrections and μ_c optimized corrections at the extinction levels $A_{K_s} = 0^m5, 1^m0, 2^m0$ and 3^m0 .

Galaxy	Param.	0^m5	<i>SDE</i>	1^m0	<i>SDE</i>	2^m0	<i>SDE</i>	3^m0	<i>SDE</i>
E/S0	$f(R)$	0.0010	0.0080	0.0025	0.0170	0.0148	0.0437	0.0623	0.0972
E/S0	Δm_{iso}	0.0004	0.0044	0.0000	0.0096	0.0037	0.0188	0.0186	0.0276
S	$f(R)$	0.0057	0.0157	0.0215	0.0449	0.2520	0.2398	2.0472	1.4042
S	Δm_{iso}	0.0022	0.0175	-0.0011	0.0388	0.0252	0.0868	0.1356	0.1451

The μ_c optimized corrections were calculated using Eqns. 9, 10.

**Figure 5.** Comparison between simulated corrections and the μ_c optimised corrections derived using $f(R, \mu_c)$ and $\Delta m_{iso}(R, \mu_c)$, top: **E/S0**, bottom: **S** galaxies.

than the corrections using the central surface brightness optimization. The better performance of μ_c in describing the corrections results from the fact that it is the outer galaxy disk that suffers more of the obscuration.

It is also worth noting that $\approx 85\%$, 94% and 98% of the galaxies in the J , H and K_s bands in our ZOA survey are in regions with an extinction $A_{J,H,K_s} \lesssim 1^m0$ where the corrections show very little dispersion.

2.3 Average behaviour (average correction)

The application of the optimized method to estimate the obscuration corrections for galaxies requires the knowledge of the value of μ_0 and hence the galaxy light profile. In many cases that information is not available, or hard to obtain, like trying to correct isophotal radii or magnitudes for galaxies in a galaxy catalogue such as the 2MASX. For such cases an average correction independent of the galaxy light profile is required. In this section we derive such an average correction. A comparison between the application of the optimized and average corrections is given later in Sect. 3.

The all elliptical galaxies and the majority of the spiral galaxies (85% of the spirals) show comparable trends (see Fig. 3), while only a few galaxies (M33, NGC24, NGC247, NGC1073, NGC55, NGC4244, marked on the plots) deviate from the average behaviour. To produce an average correction for each galaxy family **E/S0** or **S**, we excluded the strongly deviating galaxies. For the ones showing the similar behaviour (25 **E/S0** and 33 **S** galaxies) their simulated corrections were binned, resulting in an average correction curve for each family in each of the three bands. These average curves for the J , H and K_s bands are displayed in Fig. 6. For comparison the B -band corrections are displayed as well. The latter are taken from Cameron (1990).

As expected, the error bars grow with increasing extinction. It should be noted that the error bars are biased with our selection of galaxies representing the average behaviour. If we would include the strongly deviating galaxies, the error bars would obviously be larger. But given that the majority of the galaxies follow the general behaviour it would be unreasonable to include those outliers for the correction. It is also obvious from Fig. 6 that our correction curves are similar to those given by Cameron for the B band, especially the shorter J and H bands. The average correction curves were then fitted with Eqns. 4, 5. The respective fitting parameters are given in Table 6.

To gain more insight on the variation of the average correction among the galaxies, we calculated the difference between the simulated corrections and the average corrections for each galaxy

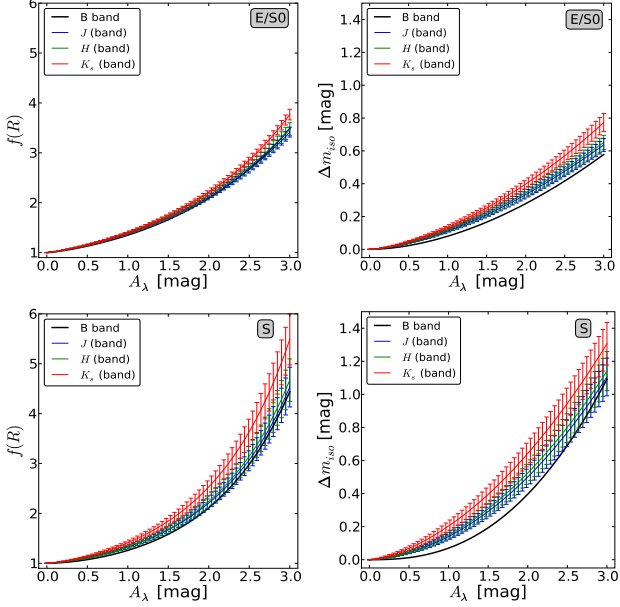


Figure 6. Average correction curves for the 25 **E/S0** (top), and 33 **S** galaxies (bottom) representing the average correction in each respective galaxy class, for the bands J , H , K_s and B band.

Table 6. Average fitting parameters a , b , F , and v for **E/S0** and **S** galaxies.

Galaxy Param.	J	H	K_s
E/S0			
a	0.1393 ± 0.0001	0.1438 ± 0.0001	0.1445 ± 0.0003
b	1.2212 ± 0.0005	1.2056 ± 0.0004	1.2555 ± 0.0018
F	0.1111 ± 0.0001	0.1175 ± 0.0002	0.1328 ± 0.0005
v	1.5872 ± 0.0008	1.5559 ± 0.0019	1.5950 ± 0.0041
S			
a	0.1169 ± 0.0007	0.1185 ± 0.0006	0.1453 ± 0.0005
b	1.5650 ± 0.0056	1.5718 ± 0.0047	1.4778 ± 0.0032
F	0.1346 ± 0.0008	0.1442 ± 0.0007	0.1982 ± 0.0009
v	1.9080 ± 0.0064	1.8755 ± 0.0053	1.7093 ± 0.0049

at $A_{K_s} = 1^m0$. The average correction was calculated using Eqns. 4, 5 and the parameters in Table 6. In Fig. 7 we plot these differences against the value of μ_0 for the galaxy in the K_s band. We find that **E/S0** galaxies with $\mu_0 \geq 16.2 \text{ mag/arcsec}^2$ and **S** galaxies with $\mu_0 \geq 16.6 \text{ mag/arcsec}^2$ are generally underestimated by the average correction, while brighter galaxies are overestimated by the correction.

To assess the accuracy of the average correction as a function of extinction, we made a comparison between the simulated corrections and those derived from the average correction in the extinction range $A_{K_s} = 0^m0 - 3^m0$. The results are plotted in Fig. 8. A summary is given in Table 7, where we list the mean difference between the simulated data and the average correction value at the extinction levels $A_{K_s} = 0^m5, 1^m0, 2^m0$ and 3^m0 , as well as their scatter.

Similar to the optimized corrections, the average correction method performs better for lower levels of extinction. Comparing Figs. 4, 5 and 8, Tables 4, 5 and 7, we notice that the optimized corrections are more accurate than the average correction method.

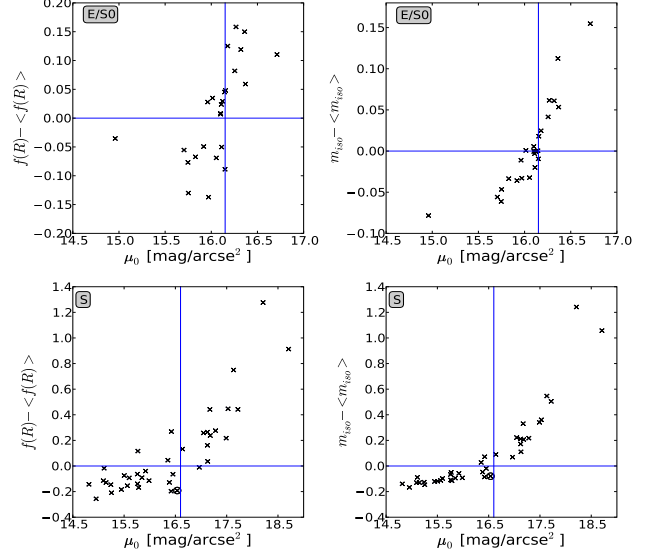


Figure 7. Difference between simulated corrections and average correction for an extinction value of $A_{K_s} = 1^m0$. Top: **E/S0**, radius correction left panel, magnitude correction right panel. Bottom: **S**, radius correction left panel, magnitude correction right panel. The values for the galaxy M88 are indicated on the spiral panels with the symbol \otimes .

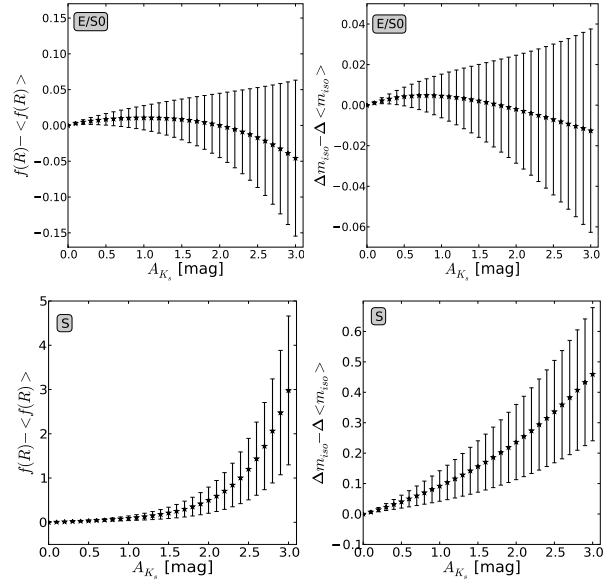


Figure 8. Comparison between simulated corrections and average corrections.

3 DISCUSSION

In this paper we present two methods to correct the isophotal magnitudes and radii for galaxies observed in the NIR obscured by foreground extinction. The optimized correction requires knowledge of the galaxy's light profile. The use of μ_c to estimate the corrections is useful as it can also be independently used to roughly categorize the galaxies as early or late type. The average correction method is more straightforward. It gives average corrections at each extinction level in the J , H , K_s observed wavebands, and only requires the classification of a galaxy as early or late type.

Table 7. Comparison between simulated corrections and the average corrections at extinction levels $A_{K_s} = 0^m.5, 1^m.0, 2^m.0$ and $3^m.0$.

Galaxy	Param.	$0^m.5$	SDE	$1^m.0$	SDE	$2^m.0$	SDE	$3^m.0$	SDE
E/S0	$f(R)$	0.0085	0.0081	0.0108	0.0170	0.0000	0.0450	-0.0457	0.1089
E/S0	Δm_{iso}	0.0425	0.0046	0.0045	0.0108	-0.0020	0.0266	-0.0126	0.0501
S	$f(R)$	0.0348	0.0177	0.0913	0.0530	0.4994	0.2961	2.9797	1.6339
S	Δm_{iso}	0.0406	0.0212	0.0920	0.0502	0.2365	0.1236	0.4594	0.2188

Average corrections were calculated using Eqns. 4, 5, and the parameters in Table 6

To compare the accuracy of the average and the μ_0 method, we used their comparison with the simulated corrections, see Figs. 4 and 8 and Tables 4 and 7. For spiral galaxies estimating the magnitude corrections using μ_0 optimization, $\Delta m_{iso}(\mu_0)$ shows a systematic shift $\Delta = -0^m.01$ with a $SDE = 0^m.0$ for an obscuration level of $A_{K_s} = 0^m.5$. Meanwhile using the average correction shows a $\Delta = 0^m.04$ with $SDE = 0^m.02$ at the same level of extinction. At $A_{K_s} = 1^m.0$, $\Delta m_{iso}(\mu_0)$ has a systematic shift of $\Delta = -0^m.01$ and a $SDE = 0^m.02$, while the average correction has a $\Delta = 0^m.09$ with a $SDE = 0^m.05$. Radius corrections for spiral galaxies revealed a similar trend for the two methods, (see Tables 4 and 7). The comparisons for the elliptical galaxies are also given in Tables 4 and 7.

Figures 4, 8 and Tables 4, 7 give the comparison between the optimized and average corrections as compared to the simulated corrections for the extinction values $A_{K_s} = 0^m.5, 1^m.0, 2^m.0, 3^m.0$. They clearly emphasize that the μ_0 optimized correction is more accurate compared to the average correction method. But the average correction remains more useful when applying the corrections to galaxy parameters from a galaxy catalogue.

The μ_c optimized correction shows larger shifts and more dispersion than the μ_0 optimized correction, but smaller shifts and tighter dispersion compared to the average correction.

In the following we give some average correction values to correct magnitudes and radii of obscured galaxies. The average correction estimates a $0^m.13$ correction to the isophotal magnitude of elliptical galaxies at $A_{K_s} = 1^m.0$. This magnitude correction is over and above the $A_{K_s} = 1^m.0$ correction. The magnitude correction shows a systematic shift of $\Delta = 0^m.01$ with a $SDE = 0^m.01$ at $A_{K_s} = 1^m.0$. As a function of radius, ellipticals are estimated to be 28.3% smaller in radius at $A_{K_s} = 1^m.0$, when using the average correction. The radius correction shows a $\Delta = 0.6\%$ and $SDE = 0.9\%$ at the same extinction level (see Table 8).

The isophotal magnitudes of spiral galaxies at $A_{K_s} = 1^m.0$ are expected to be $0^m.20$ brighter when applying the average correction. They show a systematic shift of $\Delta = 0^m.09$ with a $SDE = 0^m.05$ at $A_{K_s} = 1^m.0$. The average corrections predict that spiral galaxies appear 28.4% smaller at $A_{K_s} = 1^m.0$. The corrections show a systematic shift of $\Delta = 4.4\%$ with a $SDE = 2.6\%$ at the same obscuration level (see Table 8). The table also lists the expected magnitudes and radii corrections respectively at the extinction levels $A_{K_s} = 0^m.5, 1^m.0$ and $2^m.0$. The table also lists the systematic shifts and the SDE . The magnitude values listed in Table 8 give the additional dimming, the galaxy size reduction, the systematic shift when using the average correction and their respective SDE . The positive systematic shifts indicate that the average correction under estimates the obscuration corrections.

It is worth mentioning that our corrections agree well with

corrections given by Nagayama et al. (2004) for galaxies in the K_s band obscured by $A_{K_s} \lesssim 1^m.0$. In their work they estimated the extra dimming to elliptical galaxies to be $\Delta m_{iso} = 0^m.15$ compared to $\Delta m_{iso} = 0^m.13$ as expected by our average correction. For spiral galaxies they estimated the correction to be $\Delta m_{iso} = 0^m.18$ which also agree well with our expected correction of $\Delta m_{iso} = 0^m.20$. Compared to Nagayama et al. (2004) corrections, our results are useful for higher extinction levels in the three NIR bands J, H and K_s i.e $A_{J,H,K_s} \leq 3^m.0$.

4 CONCLUSION

We present two methods to correct galaxies for extinction in the J, H and K_s bands. The optimized correction methods are more accurate than the average correction. However the average correction method is more straightforward to apply as it requires no knowledge of the light profile of the galaxy but only the classification of galaxies as early or late types. The extinction corrections that we present here are considered as a NIR extension to those for the B band derived before by Cameron (1990).

These corrections will be invaluable to the analysis of large scale structures in the ongoing NIR galaxy survey along the Norma Wall in the ZOA. It will also be applicable to other galaxy surveys e.g. 2MASX or prospective ESO galaxy surveys e.g. VISTA Kilo-Degree Infrared Galaxy Survey (VIKING¹) using the VISTA telescope.

ACKNOWLEDGMENTS

This publication makes use of data products from the Two Micron All Sky Survey, which is a joint project of the University of Massachusetts and the Infrared Processing and Analysis Centre/California Institute of Technology, funded by the National Aeronautics and Space Administration and the National Science Foundation. The authors kindly acknowledge funding from the South African National Research Foundation. IFR acknowledges the University of Khartoum and the Stichting Steunfonds Soedanese Studenten for financial support.

The authors would also like to thank the referee for the very careful reading of the manuscript and the many remarks and comments they made to improve the overall work.

¹ <http://www.eso.org/sci/observing/policies/PublicSurveys/sciencePublicSurveys.html>

Table 8. Average magnitudes and radii corrections at $A_{K_s} = 0^m5, 1^m0, 2^m0, 3^m0$

	0 ^m 5			1 ^m 0			2 ^m 0			3 ^m 0		
[mag]	Δm_{iso}	Δ	<i>SDE</i>	Δm_{iso}	Δ	<i>SDE</i>	Δm_{iso}	Δ	<i>SDE</i>	Δm_{iso}	Δ	<i>SDE</i>
E/S0	0.044	0.004	0.005	0.133	0.005	0.011	0.401	-0.002	0.027	0.766	-0.013	0.050
S	0.061	0.041	0.021	0.198	0.092	0.050	0.648	0.236	0.124	1.296	0.459	0.219
[%]	<i>f(R)</i>	Δ	<i>SDE</i>	<i>f(R)</i>	Δ	<i>SDE</i>	<i>f(R)</i>	Δ	<i>SDE</i>	<i>f(R)</i>	Δ	<i>SDE</i>
E/S0	13.0	0.7	0.6	28.3	0.6	0.9	54.8	0.0	0.9	73.3	-0.3	0.8
S	11.3	2.7	1.4	28.4	4.4	2.6	60.6	6.5	4.1	81.7	6.5	4.3

The table lists the extra dimming and the radii reduction as estimated by the average corrections. It also lists the systematic shift Δ for comparing the simulated correction and the average correction with the respective *SDE*. The positive systematic shifts indicate that the average correction under estimate the extinction correction.

REFERENCES

Cameron, L. M. 1990, *A&A*, 233, 16
 Cardelli, J. A., Clayton, G. C., & Mathis, J. S. 1989, *ApJ*, 345, 245
 Fisher, J. R., & Tully, R. B. 1981, *ApJS*, 47, 139
 Freeman, K. C. 1970, *ApJ*, 160, 811
 Jarrett, T. N. 2004, *PA SA*, 21, 396
 Jarrett, T. H., Chester, T., Cutri, R., Schneider, S. E., & Huchra, J. P. 2003, *AJ*, 125, 525
 Jarrett, T. H., Chester, T., Cutri, R., Schneider, S., Skrutskie, M., & Huchra, J. P. 2000, *AJ*, 119, 2498
 Jarrett, T. H. 2000, *pasp*, 112, 1008
 Hauschildt, M. 1987, *A&A*, 184, 43
 Kraan-Korteweg, R. C., & Lahav, O. 2000, *A&ARV*, 10, 211
 Masters, K. L., Springob, C. M., & Huchra, J. P. 2008, *AJ*, 135, 1738
 Nagayama, T., Woudt, P.A., & Nagashima, C. et al. 2004, *MNRAS*, 354, 980
 Schlegel, D. J., Finkbeiner, D. P., & Davis, M. 1998, *ApJ*, 500, 525
 Skrutskie, M. F., et al. 2006, *AJ*, 131, 1163